



# RESEARCH MEMORANDUM

LOADS ON THIN WINGS AT TRANSONIC SPEEDS

By Don D. Davis, Jr., and Gerald Hieser

Langley Aeronautical Laboratory  
Langley Field, Va.

**NATIONAL ADVISORY COMMITTEE  
FOR AERONAUTICS  
WASHINGTON**

June 28, 1955  
Declassified July 17, 1958

NATIONAL ADVISORY COMMITTEE FOR AERONAUTICS

---

RESEARCH MEMORANDUM

---

LOADS ON THIN WINGS AT TRANSONIC SPEEDS

By Don D. Davis, Jr., and Gerald Hieser

SUMMARY

Experimental loads data at transonic speeds are reviewed in an attempt to sort out the effects of several configuration variables on the overall wing loads, and to establish the relative importance of these variables.

All plan forms show a large rearward shift of the center of pressure in the transonic speed range, but the Mach number at which this shift begins is found to be a function of such factors as taper ratio, thickness ratio, sweep angle, and the shape of the body. The center of pressure also tends to shift outboard in the transonic speed range, but this shift is found to be much larger for sweptback wings of medium taper than for highly tapered sweptback wings or for unswept or delta wings.

Wing loads measured in flight on the D-558-II airplane, which has a wing thickness ratio of about 0.09, are similar to those measured on a 6-percent-thick wing of similar sweep and aspect ratio, except that the transition from subsonic to supersonic loading characteristics begins at a lower Mach number for the thicker wing. This similarity indicates the possibility of applying these flight-test results in the structural design of thinner wings.

INTRODUCTION

Studies of aerodynamic loading at transonic speeds (for example, ref. 1) have revealed that a change in wing thickness ratio from a large value such as 0.09 to a smaller value such as 0.06 often results in large changes in wing loading characteristics. Several research programs have been conducted at the NACA for the purpose of determining the effects of configuration changes on the aerodynamic loading of thin wings (6 percent thick and less) at transonic speeds. The purpose of this paper is to summarize this information in a manner that will aid in the evaluation of the relative importance of the variables that affect wing loads. For the most part, the location of the center of loading on the wing will be used as an indicator of the overall wing loads.

## SYMBOLS

A	aspect ratio of complete wing
b	span of exposed wing
c	chord
$\bar{c}$	mean aerodynamic chord of exposed wing
$c_{av}$	average chord of complete wing
i	incidence angle
M	Mach number
P	pressure coefficient, $\frac{P - P_0}{q}$
p	local static pressure
$p_0$	free-stream static pressure
q	free-stream dynamic pressure
t/c	thickness ratio
x/c	distance along wing chord, measured from leading edge, fraction of chord
$x_{cp}$	chordwise location of center of pressure measured from leading edge of reference chord ( $\bar{c}$ or $c_{av}$ )
y	lateral distance
$y_{cp}$	spanwise location of center of pressure measured from wing- body juncture
$C_{Be}$	exposed-wing bending-moment coefficient based on exposed-wing dimensions
$C_{me}$	exposed-wing pitching-moment coefficient based on exposed-wing dimensions
$C_{Ne}$	exposed-wing normal-force coefficient based on exposed-wing dimensions

$\alpha$  angle of attack  
 $\delta_N$  nose droop angle  
 $\Lambda$  sweepback angle (subscripts .25, .30, and .50 specify reference chord line)  
 $\lambda$  taper ratio

## Subscripts:

e exposed wing  
LE leading edge

## Test designations (used in fig. 1):

F flight (including pressure measurements)  
P wind-tunnel pressure  
WB wind-tunnel wing balance

## DISCUSSION

Some of the wing-body combinations and airplanes for which wing loads data are available are represented in figure 1 (refs. 2 to 11). The symbol P in the figure signifies wind-tunnel pressure tests, and the symbol F refers to flight tests during which pressures were also measured. For the remainder of the configurations, data have been obtained from wing balances as signified by the symbol WB. The available pressure data have made it possible to study in some detail the changes in wing loading that occur in the region of transition from subsonic to supersonic speeds. However, very little detailed pressure information is included in this paper.

In figure 2, chordwise and spanwise center-of-pressure locations obtained from the data of reference 7 are plotted as a function of Mach number at a normal-force coefficient of 0.5 for two wings differing only in thickness ratio. Note that the data in this and all ensuing figures are reduced on the basis of exposed-wing geometry as indicated by the subscript e. The unusually rearward position of the wings on the research body shown in figure 2 probably has no major effect on the wing loads.

The large rearward movement of the center of pressure between Mach numbers of about 0.8 and 0.95 is due to the rearward travel of the wing shock (fig. 2). This shock reaches the trailing edge at a Mach number of about 0.95 at which speed the flow over the upper surface of the wing is almost entirely supersonic, and further increases in Mach number up to 1.2 result in only small additional movement of the center of pressure. For these thin unswept wings, the lateral position of the center of pressure is affected little by the variation of Mach number. Reducing the thickness ratio from 0.06 to 0.04 results in only a small shift of the center of pressure - rearward and outboard - and thus in only a small change in the loads. This trend exists throughout the normal-force range below the stall. Unpublished data from a different wing, for which chordwise pressure distributions were obtained at two spanwise stations, show that reducing the thickness ratio from 0.04 to 0.02 has an even smaller effect on the chordwise center of pressure than shown here.

Plots of the center of pressure for three wings with about  $35^\circ$  of sweep - a wind-tunnel model (ref. 7) and the F86-A (ref. 12) and D-558-II (ref. 8) airplanes - are shown in figure 3. Note that the center of pressure for the F-86A airplane shows a rather severe forward and inboard movement in the transonic speed range which results from a loss of lift at the tip of the wing. This characteristic has been described in the past as being typical of thick sweptback wings, because it was found that, when the thickness ratio was reduced sufficiently, the forward and inboard movement of center of pressure was eliminated. The data for the D-558-II research airplane show that the center of pressure moves rearward and outboard as the speed is increased in the transonic range, a characteristic which has been described as typical of thin swept wings. In this particular case, however, the wide difference in the behavior of center of pressure between the F-86A and D-558-II airplanes cannot be explained on the basis of wing thickness because the thickness ratios, measured streamwise, average about 0.09 for both airplanes. The differences in sweep and taper ratio are also small, but there is a significant change in aspect ratio from 3.6 for the D-558-II to 4.8 for the F-86A. Increasing the aspect ratio thus is seen to have an effect similar to that of increasing the thickness ratio, in that eventually a point is reached where further increases result in a loss in lift at the wing tips at transonic speeds with a resultant inboard and forward movement of the center of pressure. The solid lines in figure 3 indicate the center of pressure of the 6-percent-thick wind-tunnel model. The only significant difference between these curves and those for the D-558-II airplane is a delay in the Mach number at which the rearward and outboard movement of the center of pressure begins. This delay is due to the decreased thickness ratio of the wind-tunnel model which reduces the induced velocity over the wing. It is apparent from the comparison in figure 3 that the flight data from the D-558-II airplane can be used with some confidence in estimating the loads on much thinner wings of about the same plan form, whereas the F-86A data are likely to give misleading results if applied to thin wings.

In connection with the data of figure 2, it was noted that the center-of-pressure movement at supersonic speeds was relatively small for unswept wings. A similar trend is shown in figure 3 for swept wings. The flight data not only verify this trend but also show that it extends to the limit of the test data at a Mach number of 1.5. The spanwise center of pressure for the 6-percent-thick wing has been calculated at  $M = 1.2, 1.26,$  and  $1.5$  by linearized theory. The results are plotted as the diamond points and show good agreement between the theory and experiment. With decreasing supersonic Mach number, the linearized theory predicts a sizeable inboard shift of the center of loading beginning at the point where the Mach lines become parallel to the wing trailing edge - the so-called subsonic trailing-edge case. Experimentally, this shift is found to occur at subsonic rather than low supersonic speeds. If the calculations are started at the lowest Mach number for which the supersonic trailing-edge theory is applicable, and the resulting curves are simply extrapolated back to  $M = 1$ , the spanwise center of load for sweptback wings will be predicted with better accuracy than by using the theory for subsonic trailing edges.

The advantages of thin wings for high-speed flight have been clearly established from a performance standpoint. However, the choice of plan form depends to some extent on the intended mission of the airplane and therefore unswept, swept, and delta wings are all under consideration. The chordwise and spanwise center of pressure is shown in figure 4 as a function of Mach number for one of the unswept wings shown previously and also for a swept (ref. 7) and a delta wing (unpublished data) at a value of  $C_{N_e}$  of 0.5. The wings utilized here are representative of the three types of plan form, but are not necessarily optimum from a performance standpoint. Only the unswept and swept wings have the same aspect ratio, taper ratio, and thickness ratio. Although the thickness ratio of the delta wing is considerably lower than that of the other two wings, the differences shown here are primarily due to the change in plan form. Comparing the chordwise center-of-pressure location for the unswept and swept wings reveals that sweep has resulted in an increase in the Mach number at which the rearward shift of the center of pressure begins; but, at a Mach number of 1.2, the center of pressure of the two wings is in nearly the same chordwise location. The lateral center of pressure for the swept wing shows an outboard movement of about 7 percent of the exposed semispan, as Mach number is increased from subsonic to supersonic speeds. For the delta wing, the chordwise center of pressure is considerably farther rearward than for the other wings. However, because of the change in plan form the mean aerodynamic chord for the delta wing is farther inboard and considerably longer than for the other two wings, although the wing areas are the same. As a result, the rearward center-of-pressure movement with increasing Mach number for the delta wing is larger, relative to that for the other two wings, than might appear from the data of figure 4. The spanwise center of pressure

for the delta wing is located farther inboard than that for the other two wings and, like the unswept wing, it shows a much smaller movement through the transition from subsonic to supersonic flow than does the spanwise center of pressure of the swept wing.

The variation of the chordwise and spanwise center-of-pressure locations with wing normal-force coefficient for the same three wings of figure 4 is shown in figure 5. At a Mach number of 0.8, the chordwise center of pressure for the unswept wing shows a large rearward movement in the upper range of  $C_{N_e}$ , and this rearward movement is accompanied by an outboard movement. For the swept and delta wings, the inboard and forward movement of center of pressure that begins at normal-force coefficients of 0.5 to 0.8 is associated with tip stalling. This characteristic is undesirable from a longitudinal-stability standpoint and modifications incorporated to improve the stability generally delay the beginning of this center-of-pressure shift to higher normal-force coefficients. At a Mach number of 1.2, for the unswept and delta wings, the chordwise position of the center of pressure shows very little movement with increasing  $C_{N_e}$  within the range of the data. The center of pressure of the swept wing again shows a forward movement at high values of  $C_{N_e}$ . The spanwise center of pressure for the unswept wing is nearly constant at  $M = 1.2$ , whereas the swept and delta wings experience an inboard movement of the center of pressure that is similar to that shown at  $M = 0.8$ , although it is less severe. At a Mach number of 1.2, the spanwise center of pressure of the swept wing is outboard of that for the unswept wing throughout most of the range of  $C_{N_e}$ . As a result the root bending moments for the swept wing will be higher, in general, than those for the unswept wing. For example, in a maneuver at  $C_{N_e} = 0.4$  and  $M = 1.2$ , the root bending moment for the swept wing would be about 17 percent higher than for the unswept wing.

Structural considerations lead to a desire for rather highly tapered wings. Center-of-pressure locations for two swept wings identical except for taper ratio were obtained from reference 6 and are presented in figure 6. In comparing wings of different taper ratio, it is important to recognize that the mean aerodynamic chord of the more highly tapered wing is located farther inboard and is also longer. There is one chord on the wing, however, that is unaffected by a change in taper ratio; namely, the average chord of the complete wing. Consequently, the average chord has been selected as a basis for this comparison, and on this basis the change in taper ratio from 0.6 to 0.3 is found to have very little effect on the center-of-pressure location at subsonic and supersonic speeds. The transition in the transonic speed range, however, begins at a lower Mach number for the more highly tapered wing.

Some unpublished data on an even more highly tapered wing ( $\lambda = 0.15$ ) showed an outboard movement in the spanwise center of loading of less than 2 percent of the exposed semispan at transonic speeds as compared to about 7 percent for the wings shown in figure 6. The bending-moment characteristics of a very highly tapered sweptback wing thus seem to approach those of a delta wing, and the moment increase at transonic speeds is smaller than for the wings shown in figure 6. This is, of course, a favorable effect as far as the wing loads are concerned. The wing with a taper ratio of 0.15 has the same sweep and aspect ratio as the wings shown in figure 6, but it was specifically designed for efficient flight at transonic speeds and has camber and thinner airfoil sections.

At the present time, contoured bodies are being considered in the design of transonic and supersonic airplanes. In figure 7 is shown the effect of body indentation on the center-of-pressure location for a wing of aspect ratio 2.67 (unpublished data). The change in body shape is seen to result in a somewhat rearward and inboard movement of the center of pressure throughout the speed range. Tests of other wings have shown that the effect of body contouring on wing loads is less for wings of higher aspect ratio (ref. 6). This is to be expected because the effect of the body shape on the wing pressures is confined largely to the region of the wing near the body (ref. 13).

Another factor that has received increased attention recently is the use of leading-edge camber on the wings of high-speed airplanes. In order to discuss the effects of such camber on the aerodynamic loads, it is necessary to inspect chordwise pressure distributions. Pressures at the 28-percent-semispan station are shown in figure 8 for an unswept wing with the leading edge undrooped (ref. 10) and drooped  $6^\circ$  and  $10^\circ$  along the 17-percent-chord line, at angles of attack of about  $5^\circ$  and  $13^\circ$ . Pressures for the drooped cases were obtained from unpublished data. The results shown in this figure are typical of those at other spanwise stations. As the leading edge is drooped to progressively higher angles at an angle of attack of about  $5^\circ$ , the suction above the leading edge is reduced at Mach numbers of both 0.8 and 1.0. Thus, the loads on the mechanism required to droop the leading edge are highest at the breakaway point, and they can be estimated from the pressure distribution on the undrooped wing.

At a Mach number of 0.8 and an angle of attack of about  $5^\circ$ , increasing the droop results in a rearward movement of the wing shock, but behind this shock the droop has little effect on the wing loads (fig. 8). As the angle of attack is increased, the loads on the undrooped nose increase until the flow separates, at which point the loads are considerably reduced. At an angle of attack of about  $13^\circ$  and a Mach number of 0.8, the flow is completely separated at the leading edge for the  $0^\circ$  and  $6^\circ$  droop cases, but there is still a negative pressure peak at  $10^\circ$  of droop. At about the same angle of attack and a Mach number of 1.0, there is still a small

reduction in the leading-edge load as the droop is increased. Note that the trailing-edge loads are not affected by droop at either Mach number.

Unpublished results from chordwise loadings for a  $45^\circ$  swept wing with a drooped leading edge show trends similar to the unswept-wing data of figure 8.

An indication of the effect of leading-edge droop on the total wing loads is given in figure 9 which shows the pitching-moment and root-bending-moment coefficients for a swept wing with and without droop, and the root-bending-moment coefficient for the unswept wing with and without droop. The moments, rather than the center of pressure, are plotted in this figure because it is felt that they may give a somewhat clearer picture of the effect of droop. The bending moment at a constant  $C_{N_e}$  is essentially unaffected by the camber for both the swept and unswept wings, within the range of the data. Application of camber to the swept wing causes a negative increment in the pitching-moment coefficient that is nearly constant up to a normal-force coefficient of 0.4.

The effect of a change in wing incidence from  $0^\circ$  to  $4^\circ$  on the pitching-moment and root-bending-moment coefficients for a swept wing is presented in figure 10 at a Mach number of 1.0 (unpublished data). Incidence causes an essentially constant increment in the pitching and bending moments through a large part of the normal-force range. Thus, the principle of superposition of a basic loading due to incidence and an additional loading due to angle of attack is apparently valid at sonic speed as well as at subsonic speed.

#### CONCLUDING REMARKS

This discussion of experimental loads data at transonic speeds has been an attempt to sort out the effects of several configuration variables on the overall wing loads, and to establish the relative importance of these variables.

All plan forms show a large rearward shift of the center of pressure in the transonic speed range, but the Mach number at which this shift begins is found to be a function of such factors as taper ratio, thickness ratio, sweep angle, and the shape of the body. The center of pressure also tends to shift outboard in the transonic speed range, but this shift is found to be much larger for sweptback wings of medium taper than for highly tapered sweptback wings or for unswept or delta wings.

Wing loads measured in flight on the D-558-II airplane, which has a wing thickness ratio of about 0.09, are similar to those measured on a 6-percent-thick wing of similar sweep and aspect ratio, except that the transition from subsonic to supersonic loading characteristics begins at a lower Mach number for the thicker wing. This similarity indicates the possibility of applying these flight-test results in the structural design of thinner wings.

Langley Aeronautical Laboratory,  
National Advisory Committee for Aeronautics,  
Langley Field, Va., April 27, 1955.

## REFERENCES

1. Williams, Claude V., and Kuhn, Richard E.: A Study of Aerodynamic Loads on Sweptback Wings at Transonic Speeds. NACA RM L53E08b, 1953.
2. Williams, Claude V.: An Investigation of the Effects of a Geometric Twist on the Aerodynamic Loading Characteristics of a  $45^\circ$  Sweptback Wing-Body Configuration at Transonic Speeds. NACA RM L54H18, 1954.
3. Robinson, Harold L.: The Effects of Wing Incidence on the Aerodynamic Loading Characteristics of a Sweptback Wing-Body Combination at Transonic Speeds. NACA RM L54G23b, 1954.
4. Runckel, Jack F., and Steinberg, Seymour: Effects of Leading-Edge Slats on the Aerodynamic Characteristics of a  $45^\circ$  Sweptback Wing-Fuselage Configuration at Mach Numbers of 0.4 to 1.03. NACA RM L53F23, 1953.
5. West, F. E., Jr., and Henderson, James H.: Relationship of Flow Over a  $45^\circ$  Sweptback Wing With and Without Leading-Edge Chord-Extensions to Longitudinal Stability Characteristics at Mach Numbers From 0.60 to 1.03. NACA RM L53H18b, 1953.
6. Delano, James B., and Mugler, John P., Jr.: Transonic Wind-Tunnel Investigation of the Effects of Taper Ratio and Body Indentation on the Aerodynamic Loading Characteristics of a  $45^\circ$  Sweptback Wing in the Presence of a Body. NACA RM L54L28, 1955.
7. Platt, Robert J., Jr., and Brooks, Joseph D.: Transonic Wind-Tunnel Investigation of the Effects of Sweepback and Thickness Ratio on the Wing Loads of a Wing-Body Combination of Aspect Ratio 4 and Taper Ratio 0.6. NACA RM L54L31b, 1955.
8. Robinson, Glenn H., Cothren, George E., Jr., and Pembo, Chris: Wing-Loads Measurements at Supersonic Speeds of the Douglas D-558-II Research Airplane. NACA RM H54L27, 1955.
9. Kuhl, Albert E., and Johnson, Clinton T.: Flight Measurements of Wing Loads on the Convair XF-92A Delta-Wing Airplane. NACA RM H55D12, 1955.
10. Hieser, Gerald, Henderson, James H., and Swihart, John M.: Transonic Aerodynamic and Loads Characteristics of a 4-Percent-Thick Unswept-Wing-Fuselage Combination. NACA RM L54B24, 1954.

11. Jordan, Gareth H., and Hutchins, C. Kenneth, Jr.: Preliminary Flight-Determined Pressure Distributions Over the Wing of the Douglas X-3 Research Airplane at Subsonic and Transonic Mach Numbers. NACA RM H55A10, 1955.
12. Rolls, L. Stewart, and Matteson, Frederick H.: Wing Load Distribution on a Swept-Wing Airplane in Flight at Mach Numbers up to 1.11, and Comparison With Theory. NACA RM A52A31, 1952.
13. Byrd, Paul F.: Theoretical Pressure Distributions for Some Slender Wing-Body Combinations at Zero Lift. NACA RM A54J07, 1955.

WING-LOADS TESTS AT TRANSONIC SPEEDS  
 P, PRESSURES; WB, WING BALANCE; F, FLIGHT TESTS

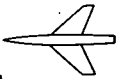
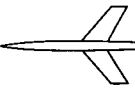
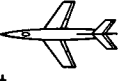
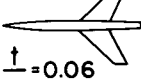
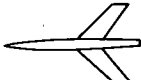
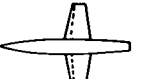
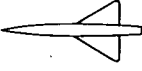
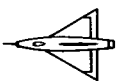
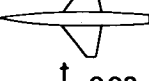
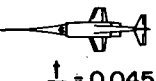
DATA		REMARKS	DATA		REMARKS
	P	BODY SHAPE		P	
$\frac{y}{b/2}$	$\frac{t}{c}$		$\frac{t}{c} = 0.04$		
0	0.06			WB	
.5	.03	WB $i = 0^\circ, 4^\circ$	$\frac{t}{c} = 0.06$		
1.0	.03	WB BODY SHAPE		F	D-558-II
	$\frac{t}{c} = 0.06$	P TWIST = $4^\circ, i = 4^\circ$	$\frac{t}{c} \approx 0.09$		
	$\frac{t}{c} = 0.06$	P L.E. DROOP = $0^\circ, 6^\circ$			
		P L.E. SLATS			
		P L.E. CHORD-EXT.			
		WB BODY SHAPE		P	L.E. DROOP = $0^\circ, 6^\circ, 10^\circ$
	WB	BODY SHAPE	$\frac{t}{c} = 0.04$		
	P	L.E. CAMBER		WB	BODY SHAPE
$\frac{t}{c} = 0.03$			$\frac{t}{c} = 0.04$		
	F	XF-92A		P	BODY SHAPE
$\frac{t}{c} = 0.065$			$\frac{t}{c} = 0.02$		
	WB			F	X-3
$\frac{t}{c} = 0.04$			$\frac{t}{c} = 0.045$		
$\frac{t}{c} = 0.06$					

Figure 1

EFFECT OF THICKNESS ON CENTER OF PRESSURE

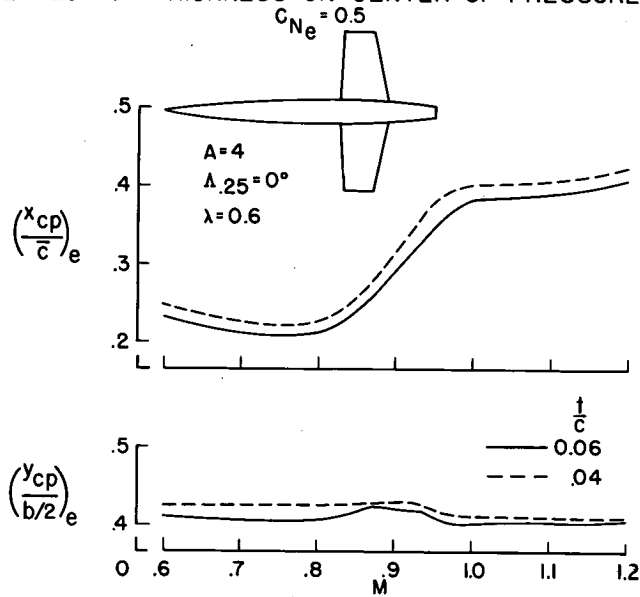


Figure 2

EFFECT OF ASPECT RATIO

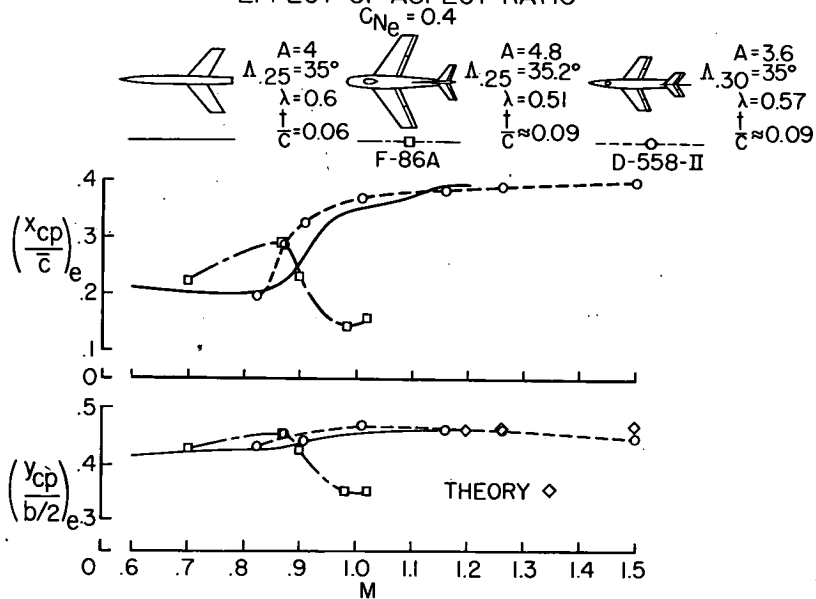


Figure 3

EFFECT OF PLAN FORM ON CENTER OF PRESSURE

$C_{Ne} = 0.5$

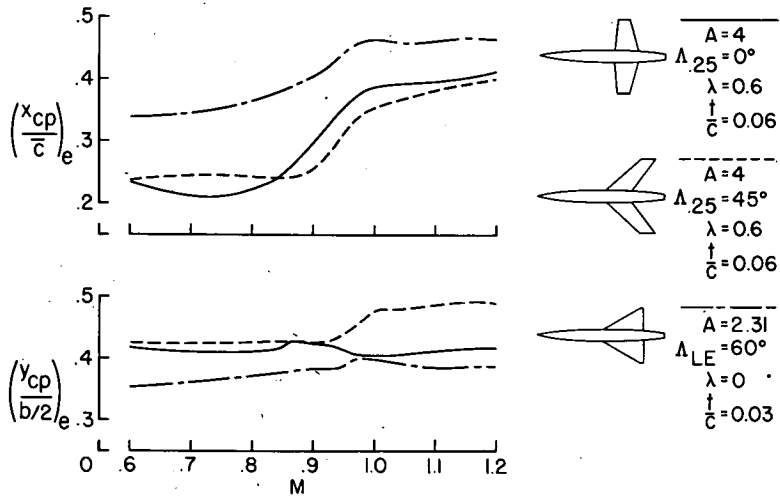


Figure 4

EFFECT OF PLAN FORM ON CENTER OF PRESSURE

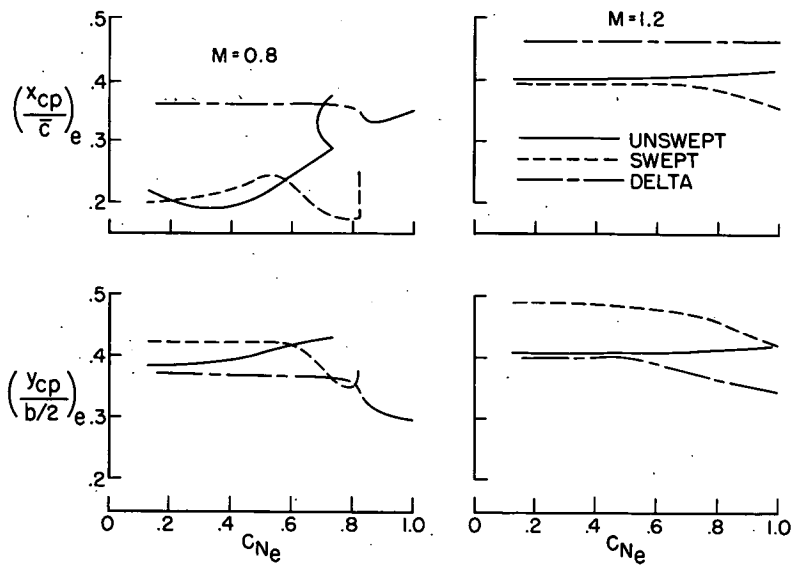


Figure 5

EFFECT OF TAPER RATIO ON CENTER OF PRESSURE

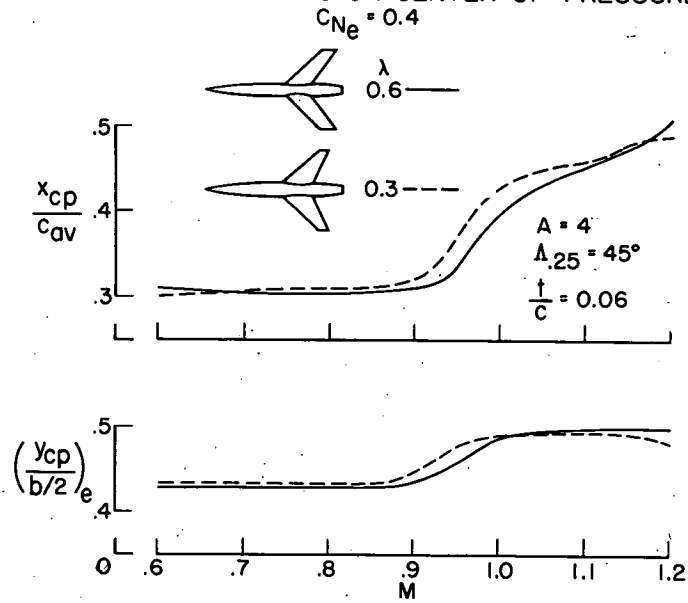


Figure 6

EFFECT OF BODY INDENTATION ON CENTER OF PRESSURE

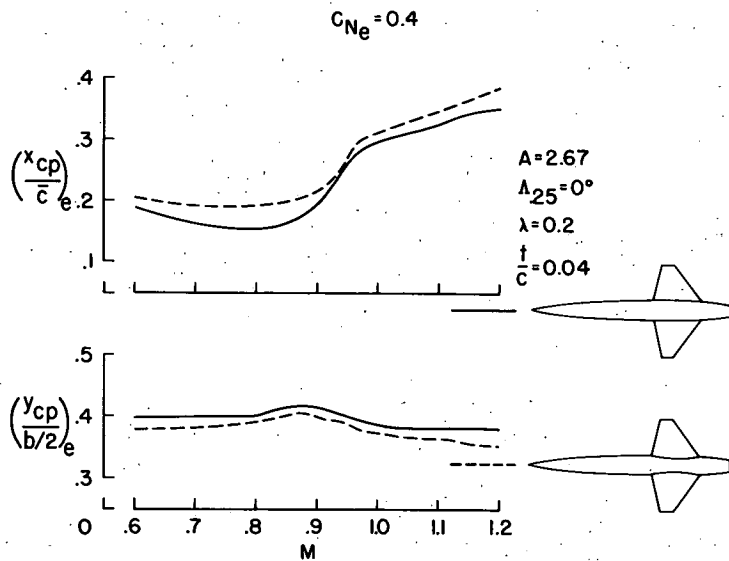


Figure 7

EFFECT OF DROOPED LEADING EDGE ON PRESSURES

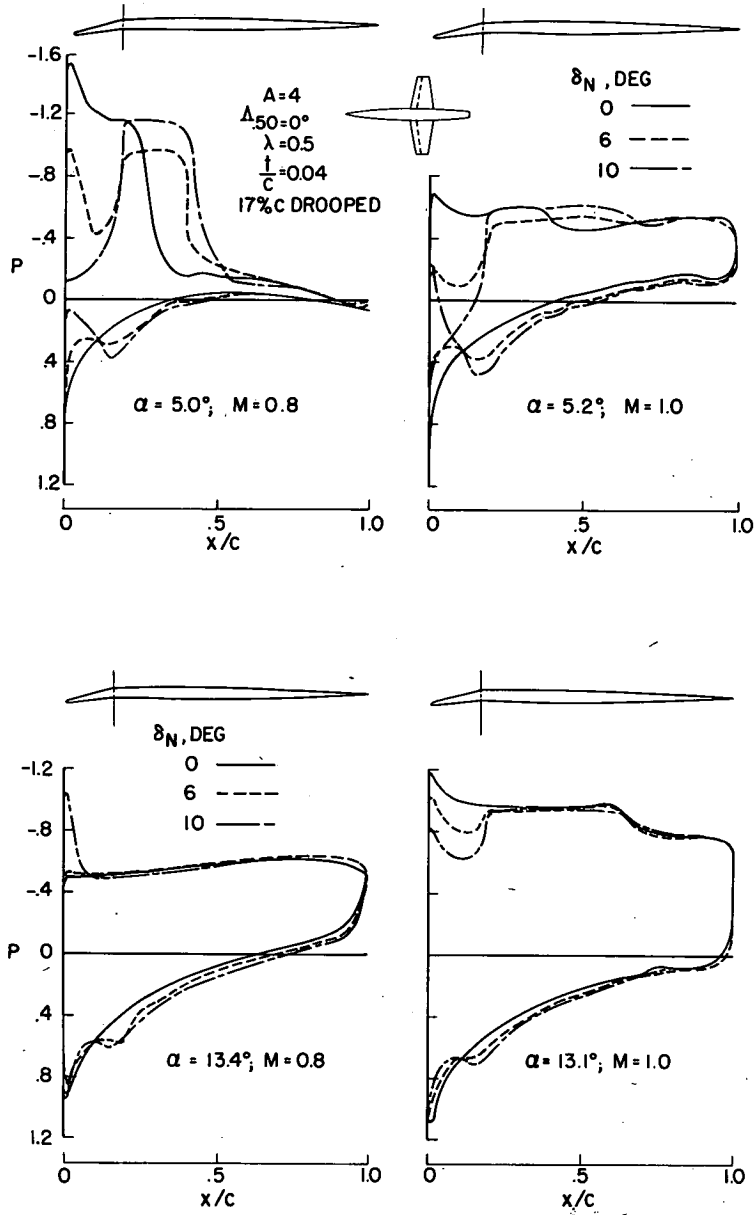


Figure 8

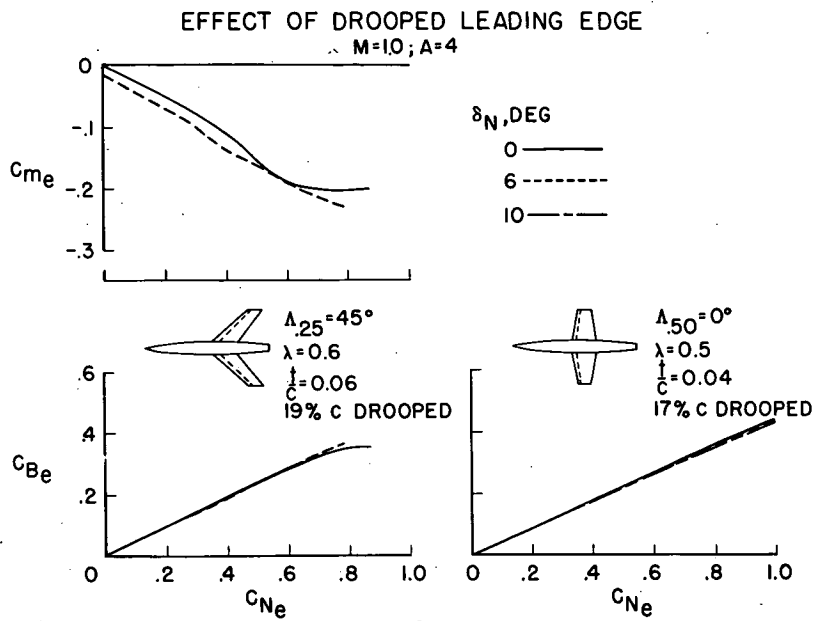


Figure 9

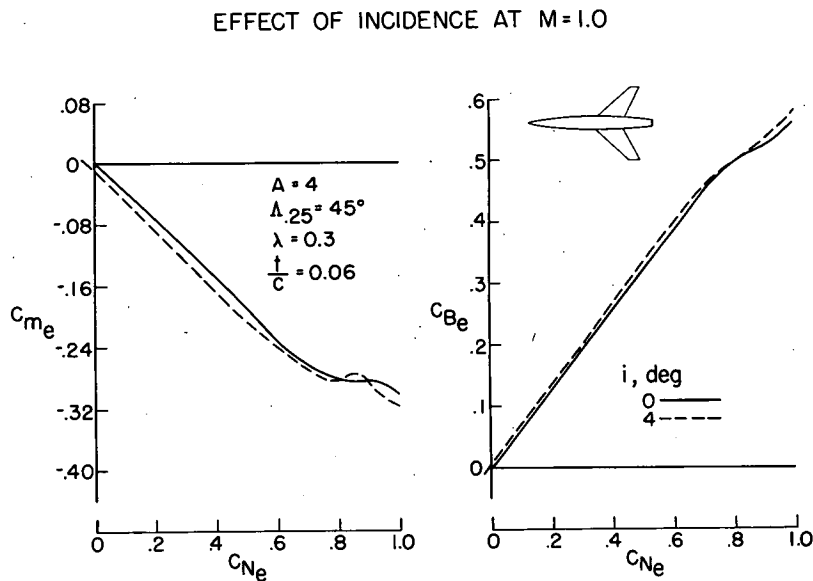


Figure 10